Spatiotemporal emission dynamics of ridge waveguide laser diodes: picosecond pulsing and switching

M. O. Ziegler

Institute of Applied Physics, Darmstadt University of Technology, Schlossgartenstrasse 7, D-64289 Darmstadt, Germany, and Fachbereich Physik and Material Science Center, Philipps-Universität Marburg, Renthof 5, D-35032 Marburg, Germany

M. Münkel, T. Burkhard, G. Jennemann, I. Fischer, and W. Elsässer

Institute of Applied Physics, Darmstadt University of Technology, Schlossgartenstrasse 7, D-64289 Darmstadt, Germany

Received March 29, 1999; revised manuscript received June 25, 1999

We report on the observation of spatiotemporal dynamics on picosecond time scales for an antireflection-coated ridge waveguide laser diode that is only 5 μm wide. Depending on the applied current, three dynamic regimes can be distinguished, showing the transition from regular to irregular spatiotemporal emission. We discuss the underlying mechanisms and develop a comprehensive understanding of this dynamic behavior. First, for moderate pumping, we find a typical relaxation oscillation behavior of the fundamental lateral mode. Second, at intermediate current levels, we observe lateral high-frequency switching of the output intensity between the left-hand and the right-hand parts of the active region. The switching frequency increases linearly with the excitation current and is of the order of 10 GHz. We give evidence that this switching behavior results from the coexistence and interaction of fundamental and first-order lateral modes that belong to different longitudinal mode families. The observed dependence of the switching frequency on the bias current can be attributed to a change in the width of the emission profile. Third, at high pumping levels, irregular spatiotemporal dynamics with the coexistence of low- and high-frequency spatial switching and temporal pulsations can be found. Finally, the influence of waveguide design and consequences for applications are considered and discussed. [S0740-3224(99)01911-6]

OCIS codes: 140.0140, 140.2020, 140.5960, 320.5390.

1. INTRODUCTION

High-power semiconductor lasers are key devices in telecommunication systems, e.g., for pumping of rare-earth-doped fiber amplifiers. Therefore narrow aluminum-free InGaAs ridge waveguide (RW) laser diodes emitting near a 980-nm wavelength have been considered in recent years to be one of the best candidates for use in such systems.[1–9] Compared with the AlGaAs system, they are less sensitive to catastrophic optical damage (COD) and therefore have increased reliability, which is essential for applications in public network systems and, particularly, in submarine transmission cables. The waveguide design is crucial for attaining not only efficient fiber coupling but also higher output power. One can achieve higher output power by enlarging the width of the active region. A width of $\sim$10 μm is regarded as the lower limit above which higher-order lateral modes and even spatiotemporal instabilities can occur. A detailed understanding of the spatiotemporal phenomena and of the relevant mechanisms is imperative for improvement of modern high-power semiconductor lasers. The best performance of pump laser diodes requires that the active area have the maximum width that will still guarantee stable lateral single-mode operation to achieve good fiber coupling. Several approaches have been developed to calculate the optimum parameters of index-guided lasers (e.g., ridge lasers) for lateral single-mode behavior.[2,10–12] However, temporally and spatially resolved model calculations are necessary to describe the spatiotemporal dynamics of those semiconductor laser devices (see, e.g., Refs. 13 and 14).

Furthermore, such a transverse optical system is of great current interest in the field of nonlinear dynamics because of the formation of spatiotemporal patterns that cover a variety of phenomena. In particular, broad-area semiconductor lasers are important model systems for the study of spatiotemporal dynamics with one relevant transverse degree of freedom.[15–20] Typical widths of broad-area semiconductor lasers range from 10 to 500 μm with an emission power of as much as several watts. However, because of the fast time scales of semiconductor laser dynamics, only a few experimental investigations with simultaneous temporal and spatial resolution have been performed. The observed spatiotemporal instabilities, which manifest themselves in irregular pulsing and dynamic filamentation, have been explained by microscopic model calculation as an interplay of self-focusing, diffraction, and spatial hole burning.[15–17]

In this paper we present experimental investigations and numerical simulations of the spatially and temporally resolved near-field emission of aluminum-free RW lasers with a ridge width of 5 μm. The results that are presented in this paper are interesting for two reasons. Knowledge of the observed spatiotemporal dynamics is imperative for the design of new laser structures because these instabilities cause a deterioration in fiber coupling of the emitted light intensity. Additionally, from the nonlinear dynamic point of view, the threshold and the phenomena at the onset of spatiotemporal instabilities are of great relevance. We concentrate on the dependence of the spatiotemporal behavior on the injection current and develop a comprehensive understanding of the underlying mechanisms by comparing the experimental data and the results of a subsequent analysis that uses methods from nonlinear dynamics with numerical model calculations. For measurement of the near field on a picosecond time scale, we used a single-shot streak camera, which has proved to be a valuable tool for the study of the dynamic behavior of semiconductor lasers.[15–17,21–23] Our simulations were carried out on the basis of laterally resolved rate equations. In what follows, we briefly describe the laser structure and laser performance and our experimental setup. In Section 3 we discuss the observed experimental and modeled spatiotemporal dynamics of the near field at several pumping levels. We also introduce and present results of eigenmode analysis. This method is a powerful tool for nonlinear dynamics that can be used to characterize the dynamics of spatiotemporal systems. Finally, we discuss the observations with respect to pumping of rare-earth-doped fiber amplifiers.

2. LASER STRUCTURE AND EXPERIMENTAL SETUP

InGaAs lasers grown upon GaAs substrates have good electrical and thermal conductivity[1] and a number of properties that are superior to those of an AlGaAs system, e.g., their low nonradiative surface recombination velocity ($<$1.5 cm/s),[24] excellent resistance to rapid degradation by propagation of dark defects,[2,24] and facet oxidation.[5] These properties yield high insensitivity to COD. The aluminum-free diode laser consists of a GaInAs quantum-well region surrounded by quaternary GaInAsP waveguides and GaInP cladding layers. The length of the laser is 1.6 mm, and the lateral width of the ridge is 5 μm. A high-reflectivity (HR) rear-facet coating (reflectivity of approximately 95%) and an antireflection (AR) front-facet coating (residual reflectivity of approximately 0.07%) yield a threshold current of $\sim$65 mA. For similar lasers with other AR–HR coatings, as reported in Refs. 1 and 3, there are no saturation effects, even in pulsed-mode operation up to the point of COD at 1200 mA with an output power of 800 mW. Thermal roll-over tests were repeated 10 times,[25] and the detected light output-versus-current curves were identical, thus demonstrating the extremely high short-term reliability against COD of these lasers. The measured far-field angles were approximately 9° $\times$ 27° FWHM ($\theta_{\parallel} \times \theta_{\perp}$), with no lateral beam-steering effects for increasing current.[1,2,7,25] Additionally, coupling tests of similar laser structures to single-mode fibers in the low-power regime (50 mW of fiber-coupled power at 180 mA) resulted in coupling efficiencies of more than 50%.[8] More-detailed descriptions of the laser structure, the growth system, and procedures can be found elsewhere.[1–3]

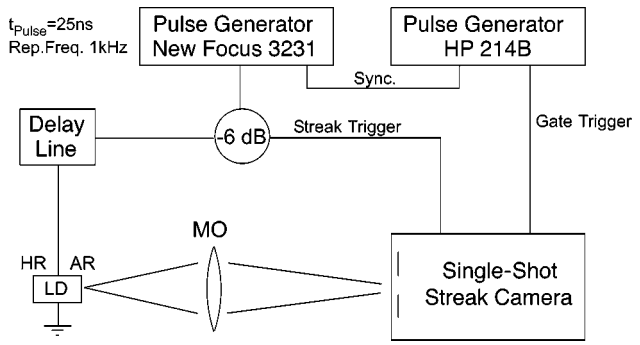

Fig. 1. Experimental setup for near-field measurements of a RW laser. MO, microscope objective; the other abbreviations are defined in the text.

The experimental setup is shown in Fig. 1. The near-field intensity distribution at the AR-coated facet of the laser diode (LD) is magnified and projected onto the input slit of a Hamamatsu C1587 streak camera with an M1952 single-sweep unit. This setup permits measurements of single-shot traces with a time resolution of as little as 10 ps, depending on the length of the selected time window. Synchronization (Sync.) of the streak camera is achieved by use of a pulse generator that supplies the RW laser via a power divider with short electrical pulses and produces a trigger signal for the camera. A second pulse generator, which is synchronized to the first one, triggers the gate of the streak camera. The laser is driven with short electrical pulses of 25 ns at a repetition frequency (Rep. Freq.) of 1 kHz and with maximum current amplitudes of 1500 mA. These values correspond to an average electrical power of less than 5 dBm and ensure that junction heating is minimized. To select the temporal position of the streak-camera traces with respect to the trigger pulse of the camera we use an electrical delay line. The traces can be read out by a CCD camera, digitally stored, and processed by a linked computer.

3. EXPERIMENTAL AND THEORETICAL INVESTIGATIONS

We have studied the dependence of the spatiotemporal dynamics on the applied current. For moderate pumping (I = 100–350 mA, corresponding to 1.5–5.4 times the threshold current), we observe the well-known relaxation oscillations that are the dynamic response of the laser to the leading edge of the injected current pulse. The observed typical relaxation oscillation behavior is confirmed by the expected linear increase of the square of the resonance frequency as a function of the intensity, however, with a saturation behavior at higher intensities, which compares well with model calculations based on rate equations including gain saturation.[23] This regime has been already studied in detail.[23] If the current is increased to intermediate pumping levels, the laser shows

regular spatiotemporal dynamics, which can be tuned by the applied current. At even higher pumping levels we find irregular spatiotemporal dynamics. These two last-named regimes, with their different spatiotemporal dynamics, are considered and discussed in what follows.

A. Regular Spatiotemporal Dynamics for Intermediate Pumping Levels ($I = 350–700$ mA)

For intermediate pumping levels of approximately 350–700 mA, corresponding to 5.4–10.9 times threshold current, we find a high-frequency switching of the output intensity between the left-hand and the right-hand parts of the active region with characteristic switching frequencies of the order of 10 GHz. Typical near-field traces for injection currents of $I = 350$ mA and $I = 550$ mA are shown in Figs. 2(a) and 2(b), respectively. The emitted intensity is linearly encoded by means of gray scales, where white corresponds to high intensity values and dark to low intensities. The near-field trace has a temporal length of 1.0 ns and shows, in accordance with the ridge of the laser, a spatial emission width of approximately 5 μm. It is striking that the switching frequency increases with increasing injection current. We measured the detailed current dependence and found a linear increase of the switching frequency with an increase of the excitation current amplitude, as shown in Fig. 2(c).

This switching between the left-hand and the right-hand parts of the active region can be observed even for longer current pulses and for long delay times of ~60 ns after the first relaxation oscillation. Even when cw current was applied, qualitatively similar switching behavior was observed. These observations prove that the sustained spatiotemporal dynamics for intermediate pumping levels is a nontransient behavior.

To model this regular spatiotemporal behavior we use laterally dependent rate equations for the complex electrical field $E(x, t)$ and the charge-carrier density $N(x, t)$. Lateral effects are introduced by lateral coupling through optical diffraction [diffraction coefficient $D_p = (1/2k_z)$, where k_z is the wave number in the propagation direction] and charge-carrier diffusion (diffusion coefficient D_f):

$$\frac{n_l}{c}\partial_t E = iD_p\partial_x{}^2 E - [\gamma_E + i\eta(x)]E + \Gamma(x)[g(N) + ik_0\delta n(N)]E, \tag{1}$$

$$\partial_t N = \Lambda(x) + D_f\partial_x{}^2 N - \gamma_{\mathrm{NR}}N - \frac{2\epsilon_0 c}{\hbar\omega_0 n_l}g(N)|E|^2. \tag{2}$$

Pump parameter $\Lambda(x)$ of the current injection via a stripe width w, the confinement factor $\Gamma(x)$, and $\eta(x) = k_0 n(x)$ with the lateral index step $n(x)$ have been provided with a rectangular lateral dependence that takes into account the stripe geometry of the laser.[13] Furthermore, γ_{NR} represents the nonradiative decay rate of the carrier density; n_l, the refractive index of the active layer; c, the speed of light; ϵ_0, the vacuum permittivity; and ω_0 and k_0, the carrier frequency and the vacuum wave number, respectively. We use the following approximations[26] for the variation of the optical gain and the refractive index of the medium with the carrier density:

$$g(N) = g_N(N - N_0), \tag{3}$$

$$\delta n = -\alpha g_N N/k_0, \tag{4}$$

with the constant linear gain coefficient g_N for all bias currents and the carrier density at transparency N_0. The linewidth enhancement factor is also assumed constant as $\alpha = 2.5$. The mirror loss is represented by the damping constant

$$\gamma_E = -\frac{\ln\sqrt{R_1 R_2}}{2L}, \tag{5}$$

where L is the length of the laser and R_1 and R_2 are the power reflectivities of the front and the rear facets, respectively. We solve the equations by assuming absorbing boundary conditions[18] in the lateral direction. The model parameters have been adapted from the experimental conditions and from the literature[2,13,14] (see Table 1).

Figure 3 shows the calculated spatiotemporal evolution of the intensity for $I/I_{\mathrm{th}} = 10$ for a time window of 50 ps.

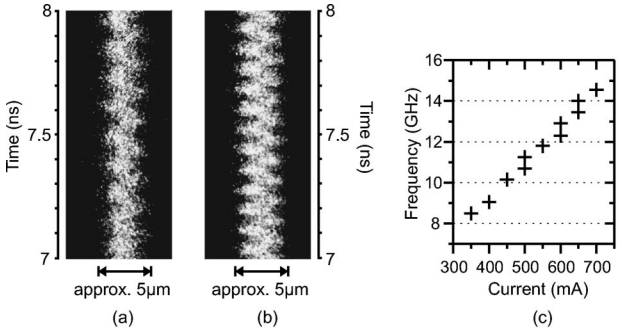

Fig. 2. Spatiotemporal near-field traces of the emitted light intensity at currents of (a) $I = 350$ mA and (b) $I = 550$ mA. The length of the time windows is 1 ns, with a delay to the first relaxation oscillation of 7 ns. (c) Dependence of the oscillation frequency on the laser current. The double plus signs indicate the spread in uncertainty.

Table 1. Parameters Used for Simulations of the Ridge Waveguide Laser

Parameter	Symbol	Value
Laser length	L	1600 μm
Stripe width	w	5.0 μm
Thickness of the active layer	d_{act}	6.0 nm
Reflectivity of the front facet	R_1	2.0×10^{-4}
Reflectivity of the rear facet	R_2	0.95
Laser wavelength	λ	975 nm
Refractive index of the active layer	n_1	3.59
Diffraction coefficient	D_p	22×10^{-9} m
Diffusion coefficient	D_f	4×10^{-4} m^2 s^{-1}
Transparency density	N_{tr}	1.8×10^{24} m^{-3}
Threshold current	I_{th}	65.0 mA
Spontaneous emission rate	B_{sp}	0.8×10^{-16} m^3 s^{-1}
Confinement factor	Γ	0.5
Alpha parameter	α	2.5

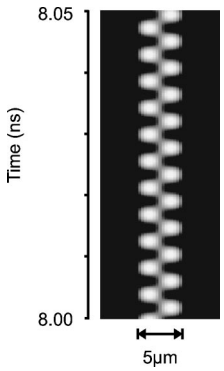

Fig. 3. Calculated spatiotemporal near field of the emitted light intensity at $I/I_{th} = 10$. The length of the time window is 0.05 ns, with a delay to the turn-on of the current pulse of 8 ns.

Compared with the measured streak-camera traces, Fig. 3 shows a qualitatively similar spatiotemporal behavior with switching between the left-hand and the right-hand sides of the active region. However, the oscillation frequency of the simulation is of the order of 230 GHz and thus approximately a factor of 20 higher than in the experimental results. This discrepancy and the origin of the switching behavior are discussed and analyzed in what follows.

To gain insight into the physical origin of the spatiotemporal switching we analyze the dynamic behavior by performing a complex eigenmode analysis of the numerical data of the calculated complex optical field amplitude. This method yields the modes of the complex optical field together with their respective oscillation frequencies, in contrast to eigenmode analysis applied to intensity traces, which permits the estimation of the system's number of degrees of freedom.[17,23]

The resultant N eigenvectors $P_j(x)$ of the complex eigenmode analysis are used for an expansion of the original complex optical field:

$$E(x, t) = \sum_j a_j(t) P_j(x), \tag{6}$$

where $a_j(t)$ are the time-dependent expansion coefficients.

The eigenvalues λ_j of covariance matrix $C_{k,l}$ are given by

$$C_{k,l} = \frac{1}{T} \int_0^T E^*(x_k, t) E(x_l, t) \mathrm{d}t, \qquad k, l = 1 \ldots N_x, \tag{7}$$

where T and N_x denote the length of the time series and the number of lateral grid points, respectively. They determine the probability of the appearance of the corresponding eigenvectors P_j in the laser output.

Figure 4(a) shows the spatial distribution of the extracted two dominant eigenmodes. The fundamental mode is symmetrical and therefore couples mainly to the center of the active region and poorly at the edges, whereas the first lateral mode is asymmetrical and reaches its maximum at $\sim 1.5\ \mu$m from the lateral center of the active region. The real eigenvalues of the covariance matrix for the two eigenmodes are $\lambda_1 = 66.4\%$ and $\lambda_2 = 33.5\%$. Thus the dynamics of the fundamental mode and the first eigenmode are the dominant contributions. The corresponding frequency spectrum, which is obtained by a fast Fourier transformation of expansion coefficient $a_j(t)$, is depicted in Fig. 4(b). It shows a frequency difference $\Delta\nu$ between the fundamental mode and the first eigenmode of $\sim$230 GHz, which corresponds to the switching frequency of the calculated temporal evolution of the intensity in Fig. 3.

Consequently, the switching can be understood as coexistence and interaction of the fundamental mode and the first lateral mode (in what follows, this is called beating). However, the numerically obtained frequency difference of the two modes, which is responsible for the switching frequency, is approximately a factor of 20 higher than the frequency observed in our experimental results. Therefore it can be excluded that the beating originates from an interaction between transverse modes that belong to the same longitudinal mode family. However, it may be that the beating transverse modes belong to different longitudinal mode families. To resolve this difficulty we measured an optical emission spectrum of the laser with a high-resolution grating spectrometer. The resolution of the spectrometer was $\sim$0.025 nm. The measured spec-

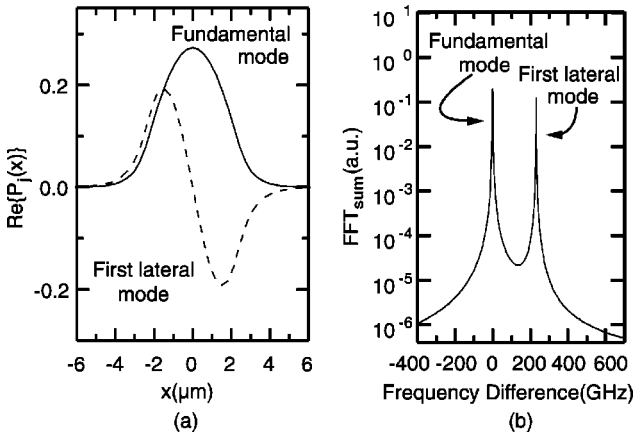

Fig. 4. (a) Real part of the eigenmodes P_j of the calculated data for the fundamental and the first lateral eigenmodes, depending on the lateral position. (b) Spectrum of the fundamental and the first lateral modes.

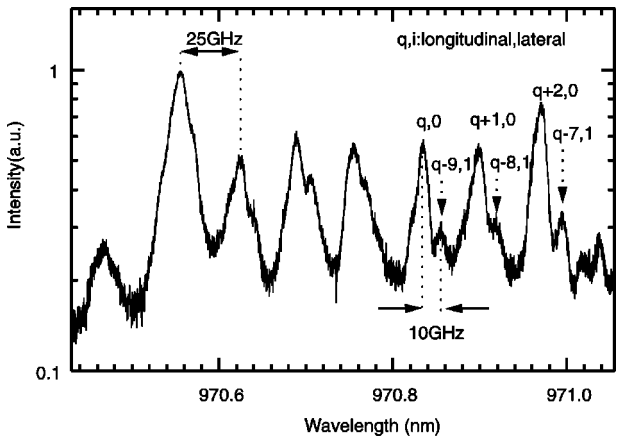

Fig. 5. Measured output spectrum at a current of $I = 500$ mA. The indices q, i of some lateral modes are shown in accordance with our theoretical calculations.

trum is depicted in Fig. 5. It shows the dependence of the spectral intensity on the wavelength for an injection current of $I = 500$ mA. It indeed reveals that the laser does not emit in a single longitudinal mode. Obviously, several longitudinal modes are excited simultaneously. The mode separation between adjacent longitudinal modes is ~25 GHz, in coincidence with the length of $L = 1.6$ mm of the laser. On the low-energy side (at higher wavelength) of each longitudinal mode we observe smaller peaks that correspond to higher-order lateral modes. Usually, first-order lateral modes have higher frequencies, because of the additional component k_x of the wave number, than the corresponding fundamental mode with the same longitudinal mode number.[27] The frequency difference from the neighboring mode of ~10 GHz corresponds to the observed spatial switching frequency. Consequently, the switching can be attributed to fundamental modes and to first-order lateral modes that belong to different longitudinal mode families, as indicated in the numbering of the modes in Fig. 5. The wavelength difference of fundamental modes and first lateral modes that belong to the same longitudinal mode family are not indicated in the spectrum, because the emission bandwidth of the investigated RW laser (the total width of the abscissa in Fig. 5 is 0.63 nm) is smaller than the calculated frequency difference of 230 GHz (corresponding to a wavelength difference of 0.7 nm). It is remarkable that we observe the beating behavior in the presence of the multiple longitudinal modes. This means that there must be phase locking among the beat frequencies that correspond to different longitudinal mode numbers, and this underlines the finding that nonlinear interaction is a key mechanism for this phenomenon. The experimental proof that, indeed, locking effects mediated by the nonlinear susceptibility of the semiconductor material[28] may make a significant contribution has already been demonstrated.[29]

After identification of the origin of the spatial switching behavior we discuss three mechanisms that can result in the dependence of the switching frequency on the injection current:

(1) The phenomenological linewidth enhancement factor α is not a device-specific constant; it shows frequency and carrier density dependence. In the center of the active region the carrier density corresponds to the threshold density even with increasing current, whereas increasingly more carriers accumulate at the edges with increasing pumping. Therefore the fundamental and the first lateral modes experience different effective values of α because of the different lateral profiles. This result is associated with a change in the refractive index and thus with a change in the frequency difference. However, these changes result in an increase in the mode separation between the fundamental mode and the first lateral mode of the same mode family with increasing current, and consequently the first lateral mode moves closer to the fundamental mode with which it is beating. Therefore this mechanism cannot explain the increase in the switching frequency.

(2) Thermal influences on the refractive index, e.g., thermal lensing, can be neglected, because of the temperature stabilization and the low duty cycle of the applied electrical pulses.

(3) Finally, lateral changes in the width of the intensity profile caused by carrier-induced changes of the waveguiding properties with increasing current can occur for these weakly index-guided ridge lasers. Therefore we have to estimate the influence of the lateral width of the emission profile. From the modeling we know that diffraction determines the frequency difference of the lateral modes and hence the switching frequency. We can roughly estimate the frequency separation of the modes by looking at the diffraction term in the rate equations [Eq. (1)]:

$$D_p \partial_x^2 E(x, t), \qquad D_p = \frac{c\lambda}{4\pi n_l \beta w^2}. \tag{8}$$

If we take into account that the electrical field vanishes at the edges of the waveguide and we assume that the first lateral mode corresponds to a half-period and the second lateral mode to a full period within the stripe width (which is normalized to 1), we obtain the wave numbers of these modes as $k_{(0)} = 2\pi \times 0.5$ and $k_{(1)} = 2\pi \times 1.0$, respectively. The diffraction term then gives a frequency separation $D_p[k_{(1)}^2 - k_{(0)}^2] \approx 230$ GHz, which should decrease with w^{-2} according to D_p.

Therefore we plot in Fig. 6 the inverse square of the width w of the experimentally measured lateral profiles as a function of the injection current. We find that w^{-2} decreases with current I, which is equivalent to a decrease in the mode separation of consecutive lateral modes with increasing current. However, because the beating occurs by interaction between different longitudinal mode families, as discussed above, this decrease in the frequency separation within one mode family is accompanied by an increase of the separation to the adjacent, different mode families, which finally results in an increase of the beating frequency, in accordance with our observations of the spatial oscillation frequency. Therefore, at least qualitatively, the tendency of an increase in the switching frequency that is obvious from Fig. 2(c) is well reproduced if we assume this mechanism.

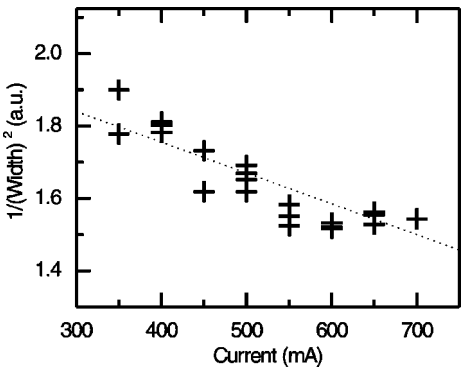

Fig. 6. Dependence of the inverse square of the width of the emission profile on the applied current for several single-shot traces. The various data points for one current indicate the spread in measurement uncertainty.

To sum up the observations in this current regime, we find that regular spatiotemporal instabilities can likely occur even for 5-μm-wide lasers. The modeling correctly describes the interaction mechanisms and the fundamental instability by means of the beating of two lateral modes. The calculated separation of fundamental and first lateral modes of 230 GHz shows up at smaller frequency differences in our experiments, because of the existing longitudinal multimode behavior. The experimentally measured switching frequency of ~10 GHz is within the relaxation oscillation bandwidth, making the occurrence of spatiotemporal dynamics more likely. To achieve a comprehensive and fully quantitative understanding of the observed instabilities of such lasers, the theoretical model must account for the various longitudinal modes by considering counterpropagating waves.[30] Further theoretical investigations are currently in progress.

B. Irregular Spatiotemporal Dynamics for High Pumping Levels ($I = 700-1500$ mA)

The laser shows irregular spatiotemporal dynamics, equivalent to a nonperiodic behavior, as depicted in Fig. 7 for $I = 1000$ mA, if the current is increased to higher pumping levels from 700 to 1500 mA, corresponding to 10.9–23.1 times threshold current.

After the occurrence of the first relaxation oscillation the light intensity starts to migrate to one side of the waveguide, as shown in Fig. 7(a). The time constant of the migration depends on the applied current and decreases from ~2 to ~0.5 ns with increasing current from $I = 700$ mA to $I = 1500$ mA. This spatiotemporal evolution dominates all single-shot traces.

Furthermore, concentrating on the time windows ~5 ns after the first relaxation oscillation, we experimentally find the coexistence of low- and high-frequency spatial switching and fast temporal pulsations [Fig. 7(b)] with frequencies up to 10 GHz. Laterally integrated time series show the irregularity of the emission for these pumping levels.

Qualitatively similar behavior can be obtained in the numerical simulations. After initial relaxation oscillations, the laser operates in the fundamental lateral mode. After some nanoseconds, however, a spontaneous symmetry breaking occurs that shows up in a gradual shift of the emission to one edge of the stripe in combination with continuously decreasing power. Having reached the respective stripe edge, the emission jumps back to the stripe center, which results in the emission of a large pulse. This process is repeated almost periodically, the characteristic period decreasing with increasing pump current, in analogy with the experimental findings. The antiguiding effect represented by the linewidth enhancement factor turns out to be responsible for this phenomenon. An accumulation of charge carriers not only provides optical gain but also causes a repulsion of the optical field because of the local decrease in the refractive index. An arbitrarily small initial displacement of the optical mode, e.g., to the left, results in a faster increase of charge carriers on the other side, here the right, of the stripe. These additional carriers at the right-hand side then result in a stronger shift of the optical mode to the left, and so on. When the optical mode has reached the left-hand stripe edge, a high carrier density has accumulated on the right-hand edge, which, finally, is depleted by a strong intensity pulse that occurs in the stripe center. This process goes on repetitively. Larger pump currents result in a faster accumulation of charge carriers, which in turn results in faster time scales for the drifting and jumping of the light emission. It is important to note that, when we chose $\alpha = 0$, no such phenomenon could be observed in the simulation. To understand the fast pulsing behavior from Fig. 7(b) we found it necessary to extend the theoretical model to multiple longitudinal modes by considering counterpropagating waves, as mentioned in Section 2.

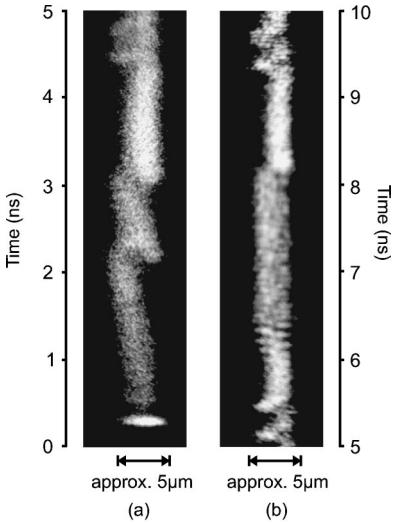

Fig. 7. Streak-camera images of the near field of the emitted light intensity for an applied current of $I = 1000$ mA. (a) Turn-on behavior, (b) 5 ns later. The length of the time windows is 5 ns.

Finally, we verified by polarization-dependent measurements that the observed spatiotemporal dynamics is not a result of polarization switching, as reported, for instance, in Refs. 31 and 32 for RW lasers. More than 95% of the emitted light is TE polarized, corresponding to the biaxial compressive strained GaInAs/InGaAsP quantum-well structure of the lasers.

4. DISCUSSION

In this paper we have shown, for the first time to our knowledge, that, in a RW laser only 5 μm broad, regular and irregular spatiotemporal dynamics can be observed. This is interesting from the point of view of nonlinear dynamics as well as for an understanding of the fundamental physics of such pump laser diodes with respect to their application. In what follows, we discuss the results of the measured spatiotemporal dynamics for moderate and high pumping levels and compare them with those of investigations reported in the literature.

For intermediate pumping levels from $I = 350$ mA to $I = 700$ mA we found that the spatiotemporal dynamics is dominated by beating of the fundamental and the first lateral modes. This type of beating of different lateral modes has been observed for other laser systems, e.g., a Nd:YAG ring laser.[33] However, in that case the spec-

trum showed no further longitudinal modes and only one fundamental and one first lateral mode. Additionally, no measurements with spatial resolution or current dependency of the oscillation frequency were reported.

Multimode behavior and mixed mode combs of fundamental and first lateral modes have been observed for GaAs–(GaAl)As, channeled-substrate planar lasers[34] with a width of the active region of 10 μm. For higher currents, even seventh-order lateral modes were observed in the time-integrated optical spectrum. Unfortunately, no time-resolved measurements of the emission or at least measurements of the electrical spectrum of the detected light were performed in the research reported in Ref. 34 to get some information about the occurrence of spatiotemporal dynamics.

We also performed investigations of RW lasers with different widths of the RW. All the lasers were processed upon one wafer, with ridge widths of 3, 4, and 6 μm and facet reflectivities of the front and rear facets of $R_1 = 95\%$ and $R_2 = 5\%$, respectively. Establishing these values allowed us to compare directly the dynamic behavior of the lasers. We found that for our structural dimensions lasers with a width of 4 μm emit in the fundamental mode, even for higher current amplitudes. For broader laser structures the occurrence of first spatiotemporal effects was observed.

Besides the ridge width, one must take further parameters into account to achieve emission in the fundamental lateral mode. In general, a trade-off among etching tolerances for the waveguide, sensitivity to carrier-induced changes of the refractive-index step, and sensitivity to high intensities on the output facet has to be made.

First, the etching depth of the ridge can significantly influence the stability of single-lateral-mode operation, as was investigated in detail in Ref. 2. On the one hand, narrow RW lasers with a waveguide width of 3 μm are easier to produce with respect to the etching tolerances for fundamental mode operation. However, narrow lasers are more sensitive to high power densities on the output facet and are thus more likely to suffer COD. On the other hand, broader ridges permit higher output power, as the power density scales almost linearly with the width,[2] but the etching tolerances for single-lateral-mode operation become smaller. Thus such ridges will more likely show a spatiotemporal pattern formation such as dynamic filamentation in the near field, which leads to a deterioration of the fiber coupling efficiency.

Second, higher carrier densities lead to a larger contribution to the refractive-index profile across the ridge. In lasers that have the same waveguide design but different cavity length, facet reflectivity, or threshold carrier density, the carrier-induced index change can even surmount the built-in index step, and the active zone of the laser becomes antiguiding. These dynamic index changes were investigated in Ref. 2 for gain-guided broad-area lasers. We have investigated a 5-μm-wide RW laser with a lower residual reflectivity of the AR-coated facet ($R = 0.02\%$) compared with the laser described in Section 3. The measured streak-camera traces showed no spatiotemporal dynamics, even for very high pumping currents up to $I/I_{\mathrm{th}} = 15$. The lower residual reflectivity leads to a higher carrier density, which reduces the built-in refractive-index step across the ridge; the laser tends to remain in the fundamental mode. This means that by tailoring the carrier density, e.g., by the parameters mentioned above, one can fine tune the index step.

To sum up with respect to applications, the ridge width, the etching depth of the ridge, and carrier-induced changes in the built-in refractive-index step are important parameters that all have to be taken into account for the occurrence of regular and irregular spatiotemporal dynamics in RW lasers. This is important for optimizing the devices, because the observed lateral instabilities obviously lead to a deterioration of the fiber coupling efficiency, which is relevant for applications such as the pumping of rare-earth-doped fiber amplifiers.

5. CONCLUSIONS

In conclusion, we have shown that, even for a ridge waveguide laser diode only 5 μm wide, spatiotemporal dynamics on a picosecond time scale can be observed. We investigated the current dependence of the dynamic behavior and found that three types of spatiotemporal emission dynamics can be distinguished.

First, at moderate pumping levels we observed the well-known relaxation oscillations that can be modeled by simple rate-equation calculations. Second, at intermediate current levels we found high-frequency switching of the output intensity between the left-hand and the right-hand parts of the active region with a frequency that increases linearly with the excitation current and is of the order of 10 GHz. We conclude from our numerical results obtained from laterally dependent rate-equation calculations and complex eigenmode analysis that this switching behavior results from beating between fundamental and lateral modes that belong to different longitudinal mode families. We have shown that calculations that incorporate lateral dependencies as well as counterpropagating waves are indispensable for modeling the complex spatiotemporal dynamics, because of the multimode behavior of such devices. Additionally, for this pumping regime we observed an increase in the width of the emission profile by which we could explain the increase in switching frequency. Finally, the third regime showed irregular spatiotemporal dynamics with the coexistence of low- and high-frequency spatial switching and temporal pulsations.

The observed spatiotemporal instabilities in the second and the third regimes, both experimentally and in simulations, are mainly the result of two effects: first, the excitation of additional spatial modes, and second, the destabilizing influence of the antiguiding effect. Both phenomena lead to spontaneous symmetry breaking of the optical emission in the lateral direction.

Our results are relevant not only for an understanding of the fundamental physical phenomena of these laser devices but also for the design of more-reliable pump laser diodes; thus they demonstrate the influence of longitudinal multimode behavior on the onset of spatiotemporal instabilities. Numerical simulations of model equations that take into account both the lateral and the longitudinal dimensions are currently in progress.

ACKNOWLEDGMENTS

The authors thank H. Asonen of Tutcore Ltd. (Finland) for providing the laser diodes and Joachim Sacher Lasertechnik (Germany) for preparing the excellent AR coatings on the laser diodes. Furthermore, we thank S. Balle, J. Martin-Regalado, and G. Erbert for valuable discussions.

REFERENCES

1. P. Savolainen, M. Toivonen, H. Asonen, M. Pessa, and R. Murison, "High-performance 980-nm strained-layer GaInAs–GaInAsP–GaInP quantum-well lasers grown by all solid-source molecular-beam epitaxy," IEEE Photon. Technol. Lett. **8**, 986–988 (1996).
2. H. Asonen, A. Ovtchinnikov, G. Zhang, J. N. Näppi, P. Savolainen, and M. Pessa, "Aluminum-free 980-nm GaInAs/GaInAsP/GaInP pump lasers," IEEE J. Quantum Electron. **30**, 415–423 (1994).
3. M. Toivonen, M. Jalonen, A. Salokatve, J. N. Näppi, P. Savolainen, M. Pessa, and H. Asonen, "All solid source molecular beam epitaxy growth of strained layer InGaAs/GaInAsP/GaInP quantum well lasers (λ = 980 nm)," Appl. Phys. Lett. **67**, 2332–2334 (1995).
4. M. Ohkubo, T. Ijichi, A. Iketani, and T. Kikuta, "980-nm aluminum-free InGaAs/InGaAsP/InGaP GRINSCH SL-SQW lasers," IEEE J. Quantum Electron. **30**, 408–414 (1994).
5. T. Ijichi, M. Ohkubo, N. Matsumoto, and H. Okamoto, "High-power cw operation of aluminum-free InGaAs/GaAs/InGaP strained layer single quantum well ridge waveguide lasers," in *Proceedings of the 12th IEEE International Semiconductor Laser Conference* (IEEE, Piscataway, N.J., 1990), pp. 44–45.
6. J. Hashimoto, I. Yoshida, M. Murata, and T. Katsuyama, "Aging time dependence of catastrophic optical damage (COD) failure of a 0.98-μm GaInAs–GaInP strained quantum-well laser," IEEE J. Quantum Electron. **33**, 66–70 (1997).
7. M. Pessa, J. Näppi, G. Zhang, A. Ovtchinnikov, and H. Asonen, "Aluminum-free 980-nm laser diodes," Mater. Sci. Eng. **21**, 2111–2116 (1993).
8. H. Asonen, J. Näppi, A. Ovtchinnikov, P. Savolainen, G. Zhang, R. Ries, and M. Pessa, "High-power operation of aluminum-free (λ = 980 nm) pump laser for erbium-doped fiber amplifier," IEEE Photon. Technol. Lett. **5**, 589–591 (1993).
9. M. Ohkubo, T. Ijichi, A. Iketani, and T. Kikuta, "Aluminum free InGaAs/GaAs/InGaAsP/InGaP GRINSCH SL-QW lasers at 0.98 μm," Electron. Lett. **28**, 1149–1150 (1992).
10. M. C. Amann and B. Steegmuller, "Calculation of the refractive index-step for the metal-cladded-ridge-waveguide laser," Appl. Opt. **20**, 1483–1486 (1981).
11. T. Ohtoshi, K. Yamagushi, C. Nagaoka, T. Uda, M. Murayama, and N. Chinone, "A two-dimensional device simulator of semiconductor lasers," Solid-State Electron. **30**, 627–638 (1987).
12. J. Buus, "The theory of dielectric slab waveguide with complex refractive index applied to GaAs lasers," in *Proceedings of the 7th European Microwave Conference* (Miller Freeman, Kent, UK, 1977), pp. 27–33.
13. M. Münkel, F. Kaiser, and O. Hess, "Spatio-temporal dynamics of multi-stripe semiconductor lasers with delayed optical feedback," Phys. Lett. A **222**, 67–75 (1996).
14. M. Münkel, F. Kaiser, and O. Hess, "Stabilization of spatio-temporally chaotic laser arrays by means of delayed optical feedback," Phys. Rev. E **56**, 3868–3875 (1997).
15. I. Fischer, O. Hess, W. Elsässer, and E. Göbel, "Complex spatio-temporal dynamics in the near-field of a broad-area semiconductor laser," Europhys. Lett. **35**, 579–584 (1996).
16. I. Fischer, O. Hess, and W. Elsässer, "Nonlinear spatio-temporal emission dynamics of broad-area laser diodes," in *A Perspective Look at Nonlinear Media: From Physics to Biology and Social Sciences*, J. Parisi, St. C. Müller, and W. Zimmermann, eds., Vol. LPN503 of Lecture Notes in Physics (Springer-Verlag, Berlin, 1998), pp. 362–369.
17. T. Burkhard, M. O. Ziegler, I. Fischer, and W. Elsässer, "Spatio-temporal dynamics of broad area semiconductor lasers and its characterization," Chaos Solitons Fractals **10**, 845–850 (1999).
18. O. Hess, *Spatio-Temporal Dynamics of Semiconductor Lasers* (Wissenschaft und Technik Verlag, Berlin, 1993).
19. O. Hess, "Spatio-temporal complexity in multi-stripe and broad-area semiconductor lasers," Chaos Solitons Fractals **4**, 1597–1618 (1994).
20. O. Hess, S. W. Koch, and J. V. Moloney, "Filamentation and beam propagation in broad-area semiconductor lasers," IEEE J. Quantum Electron. **31**, 35–43 (1995).
21. R. K. DeFrees, D. J. Bossert, N. Yu, K. Harnett, and R. A. Elliot, "Spectral and picosecond temporal properties of flared guide Y-coupled phase-locked laser arrays," Appl. Phys. Lett. **53**, 2380–2382 (1988).
22. I. Fischer, G. H. M. van Tartwijk, A. M. Levine, W. Elsässer, E. Göbel, and D. Lenstra, "Fast pulsing and chaotic itinerancy with a drift in the coherence collapse of semiconductor lasers," Phys. Rev. Lett. **76**, 220–223 (1996).
23. M. O. Ziegler, E. Miltényi, M. Münkel, J. Greif, G. Jennemann, I. Fischer, H. Asonen, and W. Elsässer, "Spatio-temporal dynamics in the near-field of a 980-nm ridge waveguide pump laser diode," in *Physics and Simulation of Optoelectronic Devices V*, M. Osinski and W. Chow, eds., Proc. SPIE **2994**, 572–579 (1997).
24. J. M. Olson, R. K. Ahrenkiel, D. J. Dunlavy, B. Keyes, and A. E. Kibbler, "Ultralow recombination velocity at $Ga_{0.5}In_{0.5}P$/GaAs heterointerfaces," Appl. Phys. Lett. **55**, 1208–1210 (1989).
25. H. Asonen, Tampere University of Technology, Tampere, Finland (personal communication, 1997).
26. G. P. Agrawal and N. K. Dutta, *Long-Wavelength Semiconductor Lasers* (Van Nostrand Reinhold, New York, 1986).
27. A. E. Siegman, *Lasers* (University Science, Mill Valley, Calif., 1986).
28. R. F. Kazarinov, C. H. Henry, and R. A. Logan, "Longitudinal mode self-stabilization in semiconductor lasers," J. Appl. Phys. **53**, 4631–4644 (1982).
29. L. K. Tiemeijer, P. I. Kuindersma, P. J. A. Thijs, and G. L. J. Rikken, "Passive FM locking in InGaAsP semiconductor lasers," IEEE J. Quantum Electron. **25**, 1385–1392 (1989).
30. M. Homar, J. V. Moloney, and M. San Miguel, "Traveling wave model of a multimode Fabry–Pérot laser in free running and external cavity configurations," IEEE J. Quantum Electron. **32**, 553–566 (1996).
31. A. Klehr, A. Bärwolf, R. Müller, M. Voss, J. Sacher, W. Elsässer, and E. O. Göbel, "Ultrafast polarization switching in ridge waveguide laser diodes," Electron. Lett. **27**, 1680–1682 (1991).
32. A. Klehr, R. Müller, M. Voss, and A. Bärwolf, "Gigahertz switching behavior of polarization-bistable InGaAsP/InP lasers under high-frequency current modulation," Appl. Phys. Lett. **64**, 830–832 (1994).
33. N. Hodgson and H. Weber, *Optical Resonators: Fundamentals, Advanced Concepts and Applications* (Springer-Verlag, London, 1997).
34. P. A. Kirkby and G. H. B. Thompson, "Channeled substrate buried heterostructure GaAs–(GaAl)As injection lasers," J. Appl. Phys. **47**, 4578–4589 (1976).